Climate Dynamics (2024) 62:10767–10783
https://doi.org/10.1007/s00382-024-07475-w

ORIGINAL ARTICLE

Summer evapotranspiration-cloud feedbacks in land-atmosphere interactions over Europe

Yikui Zhang[1,2] · **Niklas Wagner**[1,2] · **Klaus Goergen**[1,2] · **Stefan Kollet**[1,2]

Received: 14 May 2024 / Accepted: 13 October 2024 / Published online: 24 October 2024

Abstract
Land-atmosphere (L-A) feedbacks are important for understanding regional climate functioning. However, the accurate quantification of feedback strength is challenging due to complex, nonlinear interactions and varying background atmospheric conditions. In particular, the role of cloud water in the terrestrial water cycle is often ignored or simplified in previous L-A feedback studies, which overlook the relationship between evapotranspiration (*ET*) and cloud water (*TQC*). This study diagnoses the interactions between ET, TQC and its dynamics ($\Delta TQC/\Delta t$) under different atmospheric conditions by conducting correlation and a novel scaling analysis, based on a coupled regional climate model simulation. Contrasting correlation relationships between ET, TQC and $\Delta TQC/\Delta t$ were identified, indicating the positive feedback between ET and the dynamics in cloud water. Two types of positive scaling relationships between ET and $\Delta TQC/\Delta t$ were identified by K-means clustering. The analysis shows a contrasting north-south distribution of the scaling relationship that is similar to the spatial distribution of energy-limited and water-limited ET regimes, highlighting the role of ET regimes in modulating the ET - $\Delta TQC/\Delta t$ scaling relationships. Moreover, the feedback strength and scaling relationship are affected by atmospheric moisture flux dynamics, providing remote moisture sources and altering dry/wet conditions. Our results highlight the role of cloud water in the atmospheric part of the L-A process chain and reveal the effect of different atmospheric conditions on L-A interactions based on the new analysis framework.

Keywords Land-atmosphere interaction · Evapotranspiration · Cloud water · Regional climate simulation

1 Introduction

The influence of land surface moisture fluxes accounts for a substantial fraction of the simulated changes in the atmospheric water cycle in climate projections (Taylor et al. 2012; Allan et al. 2020; Zhou et al. 2021). In particular, the feedback chain between soil moisture (SM) and precipitation (Pr) through land-atmosphere (L-A) interaction attracts much attention as it connects variable surface fluxes, planetary boundary layer processes, and the free atmosphere through the Local L-A Coupling (LoCo) process chain as a result of the surface flux sensitivity to changes in land surface conditions (Dirmeyer et al. 2013a, b; Fischer et al. 2007; Santanello et al. 2011, 2018; Seneviratne et al. 2010). Koster et al. 2004 demonstrated through ensemble global climate model (GCM) simulations that, on a global scale, SM exerts a strong positive influence on Pr in transitional zones between dry and wet climates during the boreal summer. In these regions, such as the central USA, Sahelian Africa, and South Asia, evapotranspiration (ET) is both strong and highly sensitive to variations in SM. At a local scale, Findell and Eltahir 2003a, 2003b have explained the role of direct and indirect SM-Pr coupling under wet-soil or dry-soil advantage regimes through the direct moisture cycle or the modification of the planetary boundary layer (PBL) stability to trigger convection, showing either positive (more precipitation over wet soils) or negative SM-Pr coupling (more precipitation over dry soils).

However, many studies have highlighted the local relevance of large-scale atmospheric moisture flux dynamics ($AMFD$), such as the low-level jet or large-scale moisture transport, on SM-Pr coupling by providing remote

✉ Yikui Zhang
yik.zhang@fz-juelich.de

[1] Agrosphäre (IBG-3), Institute of Bio- and Geosciences, Forschungszentrum Jülich, Jülich, Germany

[2] Centre for High-Performance Scientific Computing in Terrestrial Systems, Geoverbund ABC/J, Jülich, Germany

moisture sources and modifying local boundary layer processes (Dominguez and Kumar 2008; Tao et al. 2019). Observational studies in the U.S. Southern Great Plains have shown that Pr is more closely related to moisture flux convergence than local ET; the daily atmospheric moisture balance is mainly dominated by large-scale atmospheric forcing, but the dependence can also vary under dry or wet conditions of both the land surface and the atmosphere (Phillips and Klein 2014; Tao et al. 2019). Welty and Zeng (2018) argue that the strength of the $AMFD$ can modulate the sign of L-A, such that a low morning soil moisture tends to intensify subsequent afternoon precipitation (a negative correlation) under conditions of low moisture dynamics, but can also be significantly reversed to a positive correlation under strong dynamics in US Great Plains with more precipitation over a humid land surface. Ford et al. (2015) found that in the same region, low-level jets can reduce the stability of the lower troposphere and mask the influence of local moisture by advecting warm and moist air from a distance. Meanwhile, $AMFD$ can inhibit local L-A coupling by transporting clouds from the originating dry land surface to wetter patches (Chen et al. 2020). Su et al. (2014) argue that $AMFD$ plays an important role in the development of positive ET-Pr feedback by increasing the efficiency of moisture conversion from local ET provided by wet soils to Pr. On the global scale, Qing et al. 2023 found that the SM-ET-Pr coupling chain contributes mostly to the post-drought Pr in humid regions, while the contribution of moisture flux convergence on post-drought Pr is much stronger in arid regions due to enhanced low-level flux convergence from drying soils. While $AMFD$ was also found to consistently inhibit the local L-A feedback in the Atlantic coast and Mediterranean regions (Jach et al. 2022; Schwitalla et al. 2023), a more comprehensive analysis of its effect in Europe is still lacking and requires datasets with higher horizontal resolution.

The control of SM on Pr depends on several interrelated processes, with a terrestrial leg representing the feedback between land conditions and surface fluxes, and an atmospheric leg representing the feedback between surface fluxes and atmospheric components (Dirmeyer 2011). Most attention in L-A coupling analysis has been paid to the relationship between SM and ET or Pr, while intermediate processes in the process chain, such as the feedbacks between land surface and cloud, are still elusive (Tesch et al. 2023; Wei and Dirmeyer 2012) and limited. As an important temporal storage of atmospheric moisture, clouds play an important role in controlling the land surface processes, PBL evolution, and atmospheric energy and water budgets (Betts et al. 2015; Findell and Eltahir 2003a; Sedlar et al. 2022; Tian et al. 2022). The occurrence of clouds can directly alter the surface energy budget by solar radiation reflection and absorption, resulting in a redistribution of both sensible and latent heat fluxes at the surface, which can influence the diurnal evolution of the PBL on a daily timescale by reducing the PBL height on cloudy days (Kotthaus and Grimmond 2018; Tao et al. 2019; Su et al. 2023). Ultimately, this will contribute to the dynamics of atmospheric moisture and affect convection (Berg et al. 2015; Liu et al. 2024). In addition, the influence of atmospheric conditions could also affect the local moisture flux coupling by providing remote moisture sources (Ford et al. 2015; Tao et al. 2019). Nevertheless, most of the attempts to understand interactions between clouds and land surface fluxes are limited to field observations, like the Atmospheric Radiation Measurement facility observations in the US, or reanalysis datasets, such as ERA5, which is criticized for accurately representing the coupling between clouds and the land surface (Su et al. 2024). Moreover, the role of cloud water as part of the terrestrial water cycle has often been ignored despite its contrasting role in affecting ET and land surface processes via controlling either radiation or near-surface atmospheric humidity (Berg et al. 2017; Wang et al. 2024).

This study aims to diagnose the feedbacks between ET, cloud water and cloud water dynamics under different atmospheric conditions to improve our understanding of L-A interaction by opening the black box of the feedbacks between L-A moisture fluxes. For this purpose, five atmospheric regimes based on dry/wet atmospheric conditions and the strength of the $AMFD$ were derived based on a regional climate model simulation with the fully coupled Terrestrial System Modeling Platform (TSMP) over the EURO-CORDEX 12 km domain from 1979 to 2021, in a one-way dynamical downscaling of ERA5 reanalysis forcing data. First, both correlation and scaling analyses quantify the sign and magnitude of the relationships between ET and cloud moisture dynamics. Second, the effect of different atmospheric conditions on cloud water dynamics is quantified. Finally, we try to answer two questions: what are the relationships between ET with cloud moisture, and how are their feedbacks affected by different atmospheric conditions?

2 Methodology

In this section, we introduce the setup and configuration of the TSMP regional climate system model (RCSM) and the simulation dataset, the model physics related to the L-A analysis, the dataset preprocessing, and finally the statistical L-A interaction analysis methods.

2.1 Simulation data and study area

This study used TSMP simulation results from 1979 to 2021, driven by ERA5 reanalysis (Hersbach et al. 2020) in a one-way single nest dynamical downscaling setup with prescribed daily sea surface temperature. TSMP (Shrestha et al. 2014; Gasper et al. 2014) consists of the atmospheric model COSMO (COnsortium for Small Scale MOdelling) (Baldauf et al. 2011; Doms and Schattler, 2002), the land surface model CLM (National Center for Atmospheric Research Community Land Model) (Oleson et al. 2008), and the surface-subsurface hydrologic model ParFlow (Parallel Flow) (Jones and Woodward 2001; Kollet and Maxwell 2006; Maxwell 2013), which are coupled via the OASIS3-MCT2 (Ocean Atmosphere Sea Ice Soil) coupler (Valcke 2013). The non-hydrostatic limited area numerical weather prediction model COSMO in a climate mode configuration simulates the atmospheric processes within the TSMP. COSMO provides atmospheric variables such as radiation, near-surface temperature, pressure, specific humidity, wind and precipitation to CLM3.5. The one-dimensional land surface model CLM3.5 serves as the lower boundary for the atmospheric model COSMO, which simulates the energy balance of the land surface. It also provides the soil moisture sources and sinks for the surface and subsurface model ParFlow, a three-dimensional, variably saturated surface-subsurface flow code that simulates 3D groundwater dynamics. The time step for ParFlow and CLM3.5 is 900 s, while COSMO runs with a 60 s time step. Coupling between the component models is applied at 900 s frequency with averaged values from COSMO, and the post-processed model output is 3-hourly or daily means. The TSMP simulation is an ERA5-driven follow-up to the ERA-Interim driven simulation as detailed in Furusho-Percot et al. (2019; 2022). To work with the strongest signal of L-A interaction, the analysis only considers the summer season (JJA), and daytime time values (6-21UTC) when ET is most significant (Findell et al. 2024; Phillips and Klein 2014; Tao et al. 2019). In

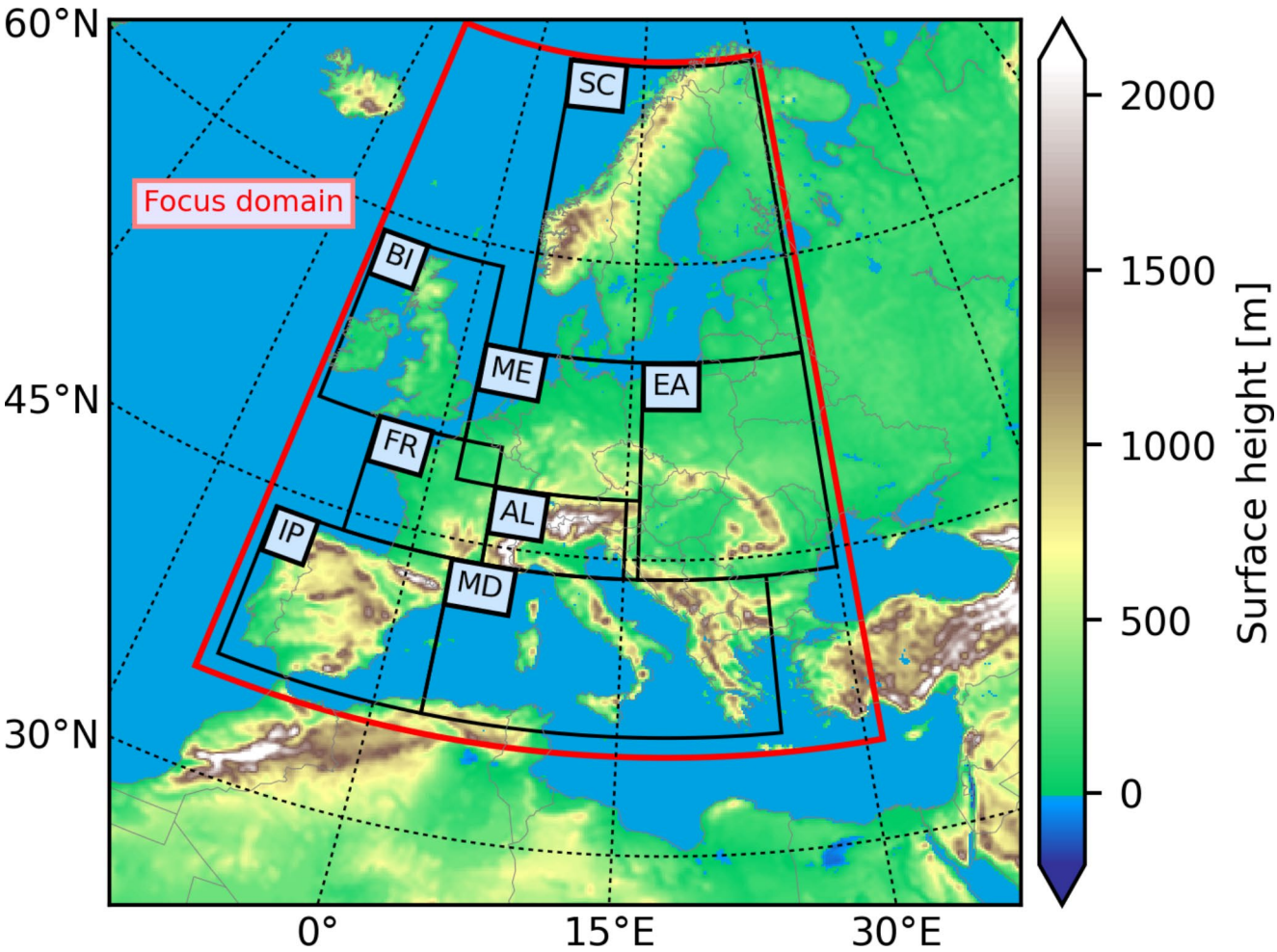

Fig. 1 TSMP simulation EURO-CORDEX domain (EUR-11, about 12 km spatial resolution, 424×412 grid elements) (red box) and PRUDENCE analysis regions (black boxes). BI: British Island; SC: Scandinavia; ME: Middle Europe; EA: East Europe; FR: France; AL: Alpine region; IP: Iberian Peninsula; MD: Mediterranean region

particular, the analysis will focus on the feedback between ET and total cloud water (TQC), representing cloud moisture. Details about the selected variables will be explained in the following section. In line with many studies on European climate, the eight PRUDENCE regions (Christensen and Christensen 2007) are used as target domains for the analysis (Fig. 1).

2.2 Moisture balance of the cloud layer in COSMO model

In an atmospheric model, such as COSMO, cloud water plays an important role in the moisture balance as a temporal storage of atmospheric moisture that represents a sink or source for local or remote moisture exchanges (Doms et al. 2021). Considering the entire atmospheric column (Eqs. 1),

$$\frac{\Delta TQC}{\Delta t} \cong -\int_{Z_s}^{Z_b} (\rho \nu \bullet \nabla q + \frac{\partial F^q}{\partial z} - Pr)dz \tag{1}$$

where TQC is the total cloud water (mm); Z_s is surface terrain height (m); Z_b is cloud top height (m); v is horizontal wind speed (m/s); q is humidity mass fraction (kg/kg); F^q is vertical turbulent flux (kg/m^2 s); Pr is precipitable water flux (kg/m^2 s); ρ is the density of horizontal moisture flux (kg/m^3). Changes in COSMO cloud moisture are related to the exchange of vertical turbulent fluxes, namely local updrafts of moisture transferred from ET and downdrafts of moisture converted to precipitation, and horizontal cloud moisture advected remotely to and from the grid point by $AMFD$, based on the cloud model in the Tiedtke Mass-Flux Scheme for cumulus parameterization during convection formation. Both local and remote moisture sources contribute to the sink or source of cloud moisture over an atmospheric column. An increase in total cloud moisture can only occur if the right-hand side of the equation is positive.

Similarly, the Warm Rain Scheme of Bulk Water-Continuity model for representing the microphysical processes of the mass fraction of hydrometeors (Eq. 2) in COSMO at individual droplets indicate that changes in cloud water mass fraction (q_c) are balanced by the rate of remote advection of cloud water mass fraction, moisture condensation from atmospheric water vapor, autoconversion, and accretion of cloud moisture to precipitable water, as shown below:

$$\frac{\partial q_c}{\partial t} \cong A_{q_c} + S_c - S_{au} - S_{ac} \tag{2}$$

where $\mathrm{q_c}$ is cloud water mass fraction (kg/kg); $\mathrm{A_{q_c}}$is advection of cloud water (kg/kg)/s; $\mathrm{S_c}$ is condensation rate (kg/kg)/s; $\mathrm{S_{au}}$ is autoconversion rate (kg/kg)/s; $\mathrm{S_{ac}}$ is accretion rate (kg/kg)/s.

At 12 km horizontal resolution, deep and shallow convection are parametrized in the COSMO model based on the Tiedtke scheme (Tiedtke 1989). Compared to other convection schemes, for example, the Tiedtke-Bechtold scheme (Bechtold et al. 2008) used in the ICON model (Zängl et al. 2015), that has been established as the next-generation model for operational weather forecasting, the Tiedtke scheme's closure assumption is based on moisture convergence, while the Tiedtke-Bechtold scheme combines both moisture convergence and convective available potential energy (CAPE) as the closure assumption. In this study, given the focus is on the atmospheric moisture balance and its relationship with land surface moisture at 12 km resolution, it is reasonable to utilize the Tiedtke convection scheme in the COSMO model. In the Tiedtke scheme, the shallow convection parameterization is activated when the moisture supply to cumulus clouds is mainly driven by the vertical fluxes (surface ET), whereas penetrative deep convection often occurs with large-scale moisture convergence. This also emphasizes the potential role of atmospheric conditions in changing the relationship between ET and cloud water, and the importance of diagnosing the individual contribution of local or remote moisture sources to the cloud formation process. Therefore, in this study, we choose simulated ET from CLM as the surface variable, and others from COSMO as atmospheric variables. In particular, cloud water is the liquid phase water in the atmosphere that is not precipitable, represented by total cloud water (TQC) as an instantaneous COSMO output at each output time step t ($i.e.\ TQC$ (t). The original output of ET from CLM is the flux during each 3-hour time interval, which was aggregated to the 3-hour sum in our analysis. Therefore, $ET\,(t)$ represents the total amount of ET in mm between the current time step t and the next time step t + 1.

In the analysis, $\Delta TQC/\Delta t$ at time step t is calculated by the difference between TQC at each 3-hour time interval at each grid element as shown in Eq. 3, where t and t + 1 are the current and next time step,

$$\frac{\Delta TQC}{\Delta t}(t) = TQC\,(t+1) - TQC\,(t) \tag{3}$$

2.3 Classification of atmospheric regimes

As the analysis includes the influence of atmospheric conditions on the coupling between ET and cloud water, the TSMP simulation results are classified into different atmospheric regimes. In the first pre-processing step, at each grid point, days with a low total cloud cover of less than 10%

are masked out to create the Baseline regime (R_{base}) of only cloudy days, relevant for the analysis in this study. For these cloudy days, to investigate the role of atmospheric aridity at the grid point scale, Dry (R_{dry}) and Wet (R_{wet}) regimes are derived based on daily total precipitation equal to 0 mm/day or greater than 0 mm/day from the R_{base} (Tao et al. 2019; Sedlar et al. 2022), to represent both, surface and atmospheric humidity. In addition, an $AMFD$ regime classification is done based on R_{base} so the $AMFD$ regimes have overlapped with R_{dry} and R_{wet}. Here, the TSMP model output moisture flux convergence is used as an indicator of the strength of atmospheric moisture flux dynamics at each grid point. A positive and negative value represents convergence and divergence, respectively. The 33rd and 66th percentiles of the absolute strength of moisture flux dynamics at each grid point are calculated based on the original dataset, and the R_{base} dataset of cloudy days is further classified into Low (R_{low}) (<33rd percentile), Medium (R_{medium}) (>33rd and <66th percentile), and High (R_{high}) (>66th percentile) moisture dynamics regimes (Welty and Zeng 2018).

2.4 Analysis methods

First, Pearson correlation coefficients were calculated between ET and $\Delta TQC/\Delta t$ *as well as*TQC to diagnose the strength of the feedback at daily resolution. Both ET -TQC and ET-$\Delta TQC/\Delta t$ correlations were calculated at a daily timescale, thus, all the 3-hour variables from Sect. 2.2 were averaged over the day for the calculation. Although it is criticized for the linear assumption in quantifying causal relationships (Tesch et al. 2023), it is acceptable to use Pearson correlation analysis in this study because we only want to derive a general characteristic of the coupling strength rather than an exact quantification. Additionally, while the correlation analysis without time lags only shows the association between two variables, a coupling mechanism can still be indirectly inferred when linked to other well-established causal relationships, as suggested by Seneviratne et al. (2010).

Also, the common L-A coupling metrics, like Pearson correlation and sensitivity index calculated based on linear slope and standard deviation Dirmeyer 2011; underestimate the non-linear nature (Wang et al. 2021) as they are only centered on evaluating the relative magnitudes of the linear relationship rather than capturing the co-variability pattern. Therefore, in this study, we use a bin-averaged scaling analysis as a second method to estimate and visualize the overall relationship between two variables (X and Y, as ET and $\Delta TQC/\Delta t$ or TQC, respectively) and to describe their nonlinear functional relationship. It is conducted at a 3-hour resolution for each grid point as neglecting short-term effects could underestimate strong diurnal variations of many land surface processes (Findell et al. 2024; Wang et al. 2024). The ET-TQC scaling was established between the total amount of ET (ET(t) during each 3-hour interval and the instantaneous TQC at the end of that interval (TQC(t+1). In this context, the time lag between ET and TQC establishes a directional relationship from land surface to the atmosphere. Similarly, the ET-$\Delta TQC/\Delta t$ scaling was applied between the total amount of ET and the changes in TQC over each 3-hour interval. As discussed in Sect. 2.2 on microphysics equations, ET can directly contribute to changes in total cloud water ($\Delta TQC/\Delta t$), which is captured by the coupling between the CLM and COSMO models operating every 900 s from the land surface to the atmosphere. Although the 3-hour output resolution may smooth this coupling effect, it still reveals an inherent lagged relationship, suggesting a coupling from ET to $\Delta TQC/\Delta t$

To establish the scaling relationship, 20 bins are created based on the value of X, and the same number of data points are ensured in each bin. The values of Y are grouped into the bins and averages are calculated for each bin based on the grid point for all JJA seasons in the dataset combined. Then, a locally weighted scatterplot smoothing (LOWESS), or moving regression, is applied to obtain the smoothed scaling curves along all the binned data points by calculating the local regression to represent their co-variability. Furthermore, K-means clustering was applied to the calculated scaling curves at each grid point to classify the types of scaling. Before doing the clustering, a dynamic time-warping algorithm was used to calculate the similarity between the smoothed scaling curves. The values of $\Delta TQC/\Delta t$ were first normalized to ensure a fair comparison in the shape of scaling curves. The optimal number of clusters was selected based on visual selection from 2 to 10 clusters since the calculation of commonly used silhouette scores was extremely computationally demanding due to our large dataset with a grid point-based analysis.

As a third method, the co-variability of $\Delta TQC/\Delta t$ with the two types of moisture sources, namely ET and the atmospheric moisture flux divergence, $TDIV\_HUM$, is then diagnosed based on the quantile-phase plot at each PRUDENCE region at a 3-hour resolution (Liu et al. 2020). The percentiles of ET and $TDIV\_HUM$ are calculated over all grid points from 1990 to 2021 and divided into 20 percentile bins (5% for each bin). The corresponding mean TQC values are then calculated in each bin to visualize the joint distribution of ET and $TDIV\_HUM$, and the joint effect of ET and $TDIV\_HUM$.

Seneviratne et al. (2010) suggested that the terms coupling, feedback, and interaction should be used more consistently and carefully to avoid confusion. In our analysis, we use the term feedback to describe the two-way interaction

between variables identified through correlation analysis, while coupling refers to the one-way relationship inferred from the lagged scaling analyses. It is important to note, however, that the feedbacks identified here do not necessarily imply causal directions. Thus, the term L-A interaction is used more broadly to describe general processes at the interfaces between land and atmosphere without implying any direction, including both one-way and two-way relationships.

3 Results

3.1 Evapotranspiration-cloud water content correlation

To diagnose the strength of L-A feedbacks, we examine the relationship between surface and atmospheric variables. In this study, our focus is on the feedbacks between ET and cloud water over the EURO-CORDEX domain under different atmospheric regimes. Figure 2 shows the strength of the feedback between daily ET and TQC. A consistently negative correlation is observed over most of the study area under all atmospheric regimes. The strongest negative feedback is preferentially found in FR, SC, BI, ME, SC and northern IP, i.e. the western Atlantic coastal region, while a relatively weak feedback is found in MD, EA and southern IP. Interestingly, the weakly correlated regions correspond to those where latent heat flux (LH) and sensible heat flux (SH) are also negatively correlated as shown in Fig. S1 in Supplementary Information (SI). Also, the absolute value of the correlation coefficients under R_{dry} is much smaller than under R_{wet}, even close to 0 in the MD coastal and SC mountain regions. The differences in the three $AMFD$ regimes are also evident in that the negative correlation coefficient generally decreases with increased moisture dynamics.

However, when looking at the correlation between ET and the dynamics of cloud moisture ($\Delta TQC/\Delta t$) in Fig. 3, it shows a predominantly positive feedback between these two variables. For R_{base}, the positive feedback is rather weak with an average correlation coefficient of less than 0.1 over the entire model domain and almost no correlation in the southern IP, MD coastal and SC mountains regions. In contrast, for R_{dry}, much higher correlation coefficients are found in EA, ME, the northern coast of IP, the AL mountains and the interior of the MD region. For R_{low} and

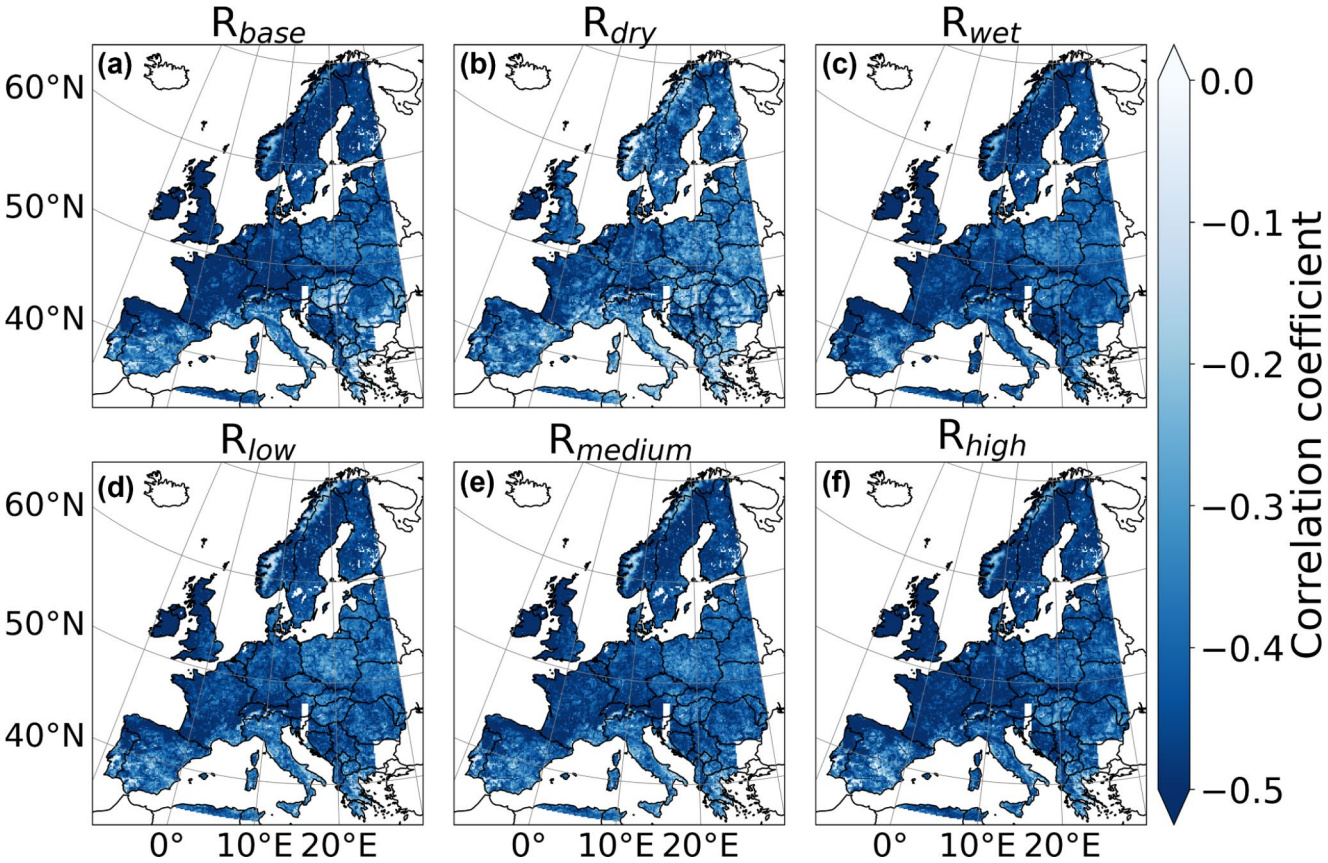

Fig. 2 Pearson correlation coefficient between daily total ET and TQC in summer (JJA) under different atmospheric conditions over the EURO-CORDEX region: (**a**) Baseline regime (R_{base}); (**b**) dry regime (R_{dry}); (**c**) wet regime (R_{wet}); (**d**) low moisture dynamic regime (R_{low}); (**e**) medium moisture dynamic regime (R_{medium}); (**f**) high moisture dynamic regime (R_{high})

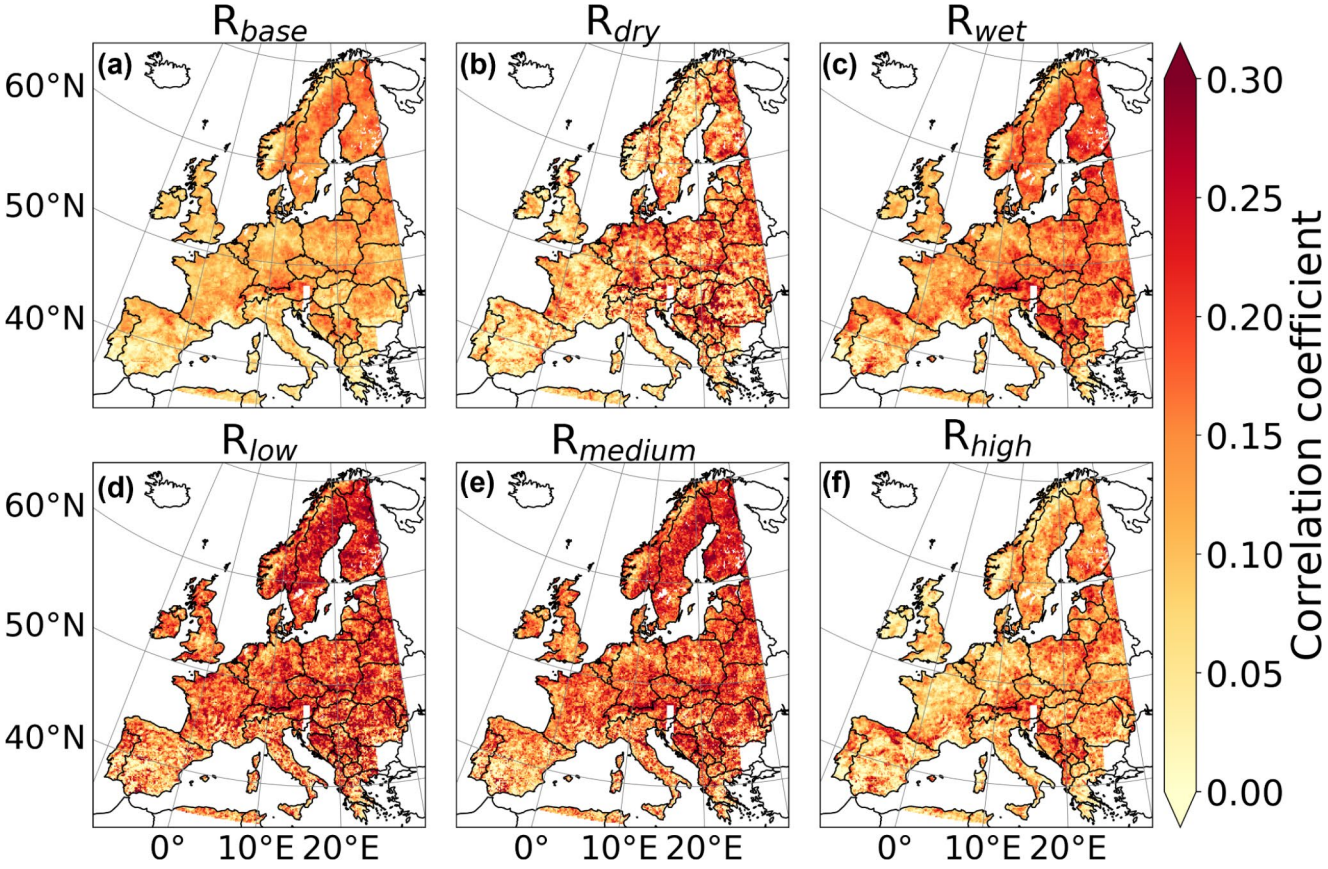

Fig. 3 Same as Fig. 2 but for ET and $\Delta TQC/\Delta t$

R_{medium}, a widespread higher positive correlation between ET and $\Delta TQC/\Delta t$ can be detected in most PRUDENCE regions, but for high moisture dynamics, R_{high}, the correlation coefficient values are significantly reduced to less than 0.1, especially in regions along the Atlantic coast, which is strongly influenced by the oceanic inflow of moist air. The larger variation in correlation coefficients between different dynamical regimes hints that the effect of $AMFD$ on the ET-$\Delta TQC/\Delta t$ feedback is more pronounced than the impact of precipitation (R_{dry} vs. R_{wet}). A notable exception is the mountainous regions in SC, which consistently show a low correlation. This could be attributed to the low ET in those regions, even in summer, as the correlation-based metrics are only meaningful when ET is relatively high (Seneviratne et al. 2006).

3.2 Evapotranspiration-cloud water content scaling

In Fig. 4, the 3-hourly binned scaling relationship between ET and TQC further confirms the negative relationship as shown by the decreasing scaling curves in all regimes, although the slopes of the scaling curves are rather small or even show a slight increase at low ET in ME, SC, AL, MD, and EA. Also, a higher sensitivity of TQC to ET is observed under both R_{wet} and R_{high} moisture dynamic regimes with a steeper declining slope, while the lowest sensitivity is under R_{dry} for all PRUDENCE regions. There is only a small difference between the curves under R_{low} and R_{medium}, but both have a steeper slope than the curves of R_{dry}.

In Fig. 5, the binned scaling curve analysis at 3-hour resolution per grid point also shows a clear positive scaling relationship between ET and $\Delta TQC/\Delta t$. However, it is subject to a certain range of ET in all PRUDENCE regions and all atmospheric regimes or conditions. A consistently positive relationship can be observed when ET is in the range of 0.2 to 0.7 *mm/3h*, while at high ET rates greater than about 0.7 *mm/3h*, $\Delta TQC/\Delta t$ tends to be insensitive to ET, showing a flat or even slightly decreasing curve. Interestingly, the scaling curves for the IP, AL, MD, and EA regions show a clear hook scaling behavior, i.e., ET and $\Delta TQC/\Delta t$ are negatively scaled at low ET values. Under R_{dry}, this hook scaling relationship is more prevalent in most of the PRUDENCE regions except for BI. The two types of scaling curves are even more obvious to be observed from the scaling curves fitted at individual grid points as shown in Fig. S2. However, the spatially averaged scaling curve in Fig. 5 only represents the dominant type of scaling and there is a clear mixture of the two types of scaling curves in

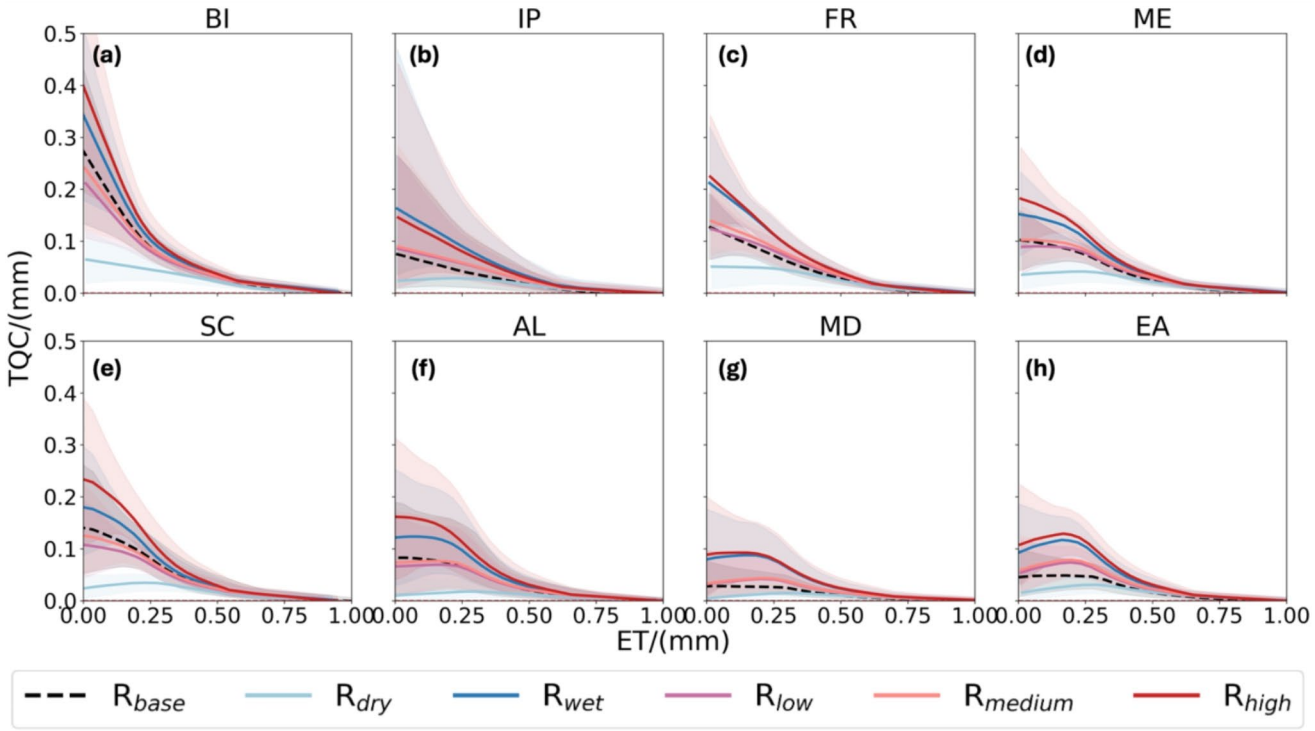

Fig. 4 The mean binned scaling curves between 3-hourly total ET and 3-hourly instant TQC under different atmospheric regimes for each PRUDENCE region from (**a**) to (**h**). Each line represents one type of atmospheric regime: Baseline regime (R_{base}) (Black dashed line); Dry regime (R_{dry}) (Light blue line); Wet regime (R_{wet}) (Dark blue line); Low moisture dynamic regime (R_{low}) (Purple line); Medium moisture dynamic regime (R_{medium}) (Orange line); High moisture dynamic regime (R_{high}) (Red line). The corresponding shading color represents the range between the 5% and 95% percentiles of the TQC at each line

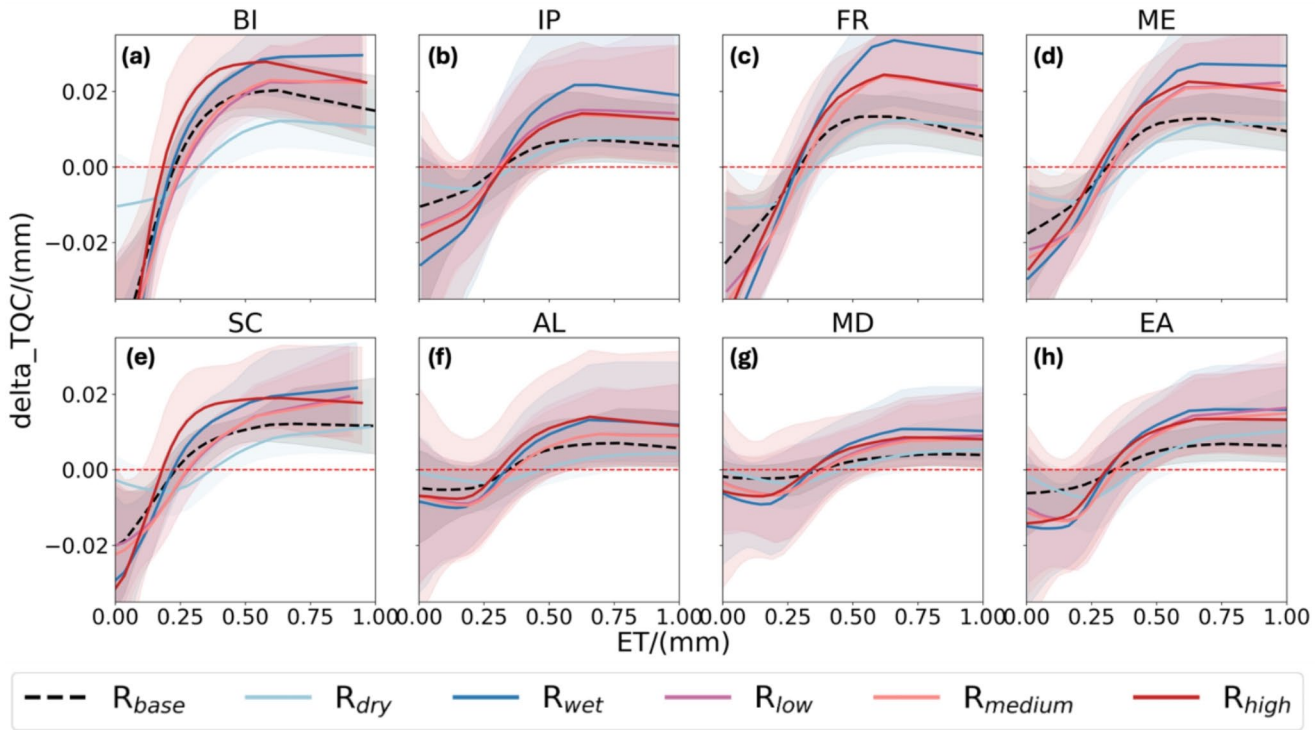

Fig. 5 The same as Fig. 4 but for ET and $\Delta TQC/\Delta t$ at each 3-hour interval. The red dashed line indicates zero $\Delta TQC/\Delta t$. The shading represents the range between the 5% and 95% percentiles of the $\Delta TQC/\Delta t$ at each line

IP, MD, EA, and AL in Fig. S2 in SI, which can be further observed in Fig. 6.

Similar to the ET-TQC scaling in Fig. 4, the slope of the scaling curves and the maximum $\Delta TQC/\Delta t$ in Fig. 5 are much smaller under R_{dry} than under R_{wet}. In contrast to the differences in the R_{dry} and R_{wet}, and the clear contrasts in the correlation coefficient values between the three moisture dynamics regimes in Fig. 3, the variation in the shape and scale of the scaling curves between different moisture dynamics regimes in Fig. 5 is very small, and only in AL and SC, the ET-$\Delta TQC/\Delta t$ scaling converge to the maximum under R_{low} under higher ET Hence, dry or wet conditions are likely to be key factors in determining the type of scaling curves. Furthermore, although ET and $\Delta TQC/\Delta t$ are positively scaled, small ET values are always associated with negative TQC dynamics, namely an intensified decrease in cloud water. This indicates that at low ET, the positive coupling cannot ensure an increase in TQC when ET is growing, as other potential sources or sinks of cloud moisture can counteract the positive local moisture contribution and lead to a depletion of TQC, which is further explained in the Discussions in Sect. 4.

We further applied the K-means clustering algorithm across all atmospheric regimes to classify the types of scaling curves at each grid point based on the shape of the scaling curves, which indicates the different responses of $\Delta TQC/\Delta t$ to changes in ET. As shown in Fig. 6 and Fig. S3, two dominant types of scaling curves have been consistently identified over all the regimes. Cluster 1 (Fig. 6a) describes the relationship between $\Delta TQC/\Delta t$ and ET as a proxy for a logarithmic function, with a gradually reduced increasing trend, while cluster 2 (Fig. 6b) represents the hook scaling relationship, with a combination of negative scaling at low ET and then logarithmic scaling. The spatial distribution of the two clusters has been visualized in Fig. 7 and shows a clear north-south contrasting spatial pattern. Under R_{base}, most of the grid points with hook scaling are located in southern Europe, especially in the Mediterranean coastal regions, including the eastern IP, MD, and southern EA regions. The logarithmic scaling appears preferentially in the Atlantic coastal regions, including western IP, FR, BI, SC, and ME. The spatial pattern is also consistent under either R_{wet} or different moisture flux dynamic regimes (R_{low}, R_{medium}, R_{high}). An exception is R_{dry}; here more grid points with hook scaling can be detected in SC, FR, ME and even BI. This can also be observed in Fig. 5 and Fig. S3 in the mean scaling curves for the IP, FR, ME, and SC regions, which all feature hook scaling.

3.3 Quantile phase diagnosis between evapotranspiration and AMFD

From Fig. 8, it is clear that from low to high ET percentiles, the increase in $\Delta TQC/\Delta t$ consistently occurs under a higher moisture flux convergence condition (indicated by lower $TDIV\_HUM$ percentile), while significant TQC depletion (negative $\Delta TQC/\Delta t$) is associated with a strong divergence (high $TDIV\_HUM$ percentile), especially when ET is in the low percentile. Looking at the relationship between ET and $\Delta TQC/\Delta t$, it is interesting to observe two types of scaling relationships as in Fig. 6. The logarithmic scaling occurs under the condition of moisture flux convergence. In contrast, hook scaling develops when the moisture flux diverges, and this type of scaling is most pronounced under R_{dry}. In the southern and eastern PRUDENCE regions (SC, AL, MD, and EA) a hook scaling can be observed under moisture flux divergence under R_{wet}, while as shown in Fig. S4, hook scaling can also be observed under R_{low}, R_{medium},R_{high} in the SC, AL, MD, and EA regions when there is strong moisture flux divergence. This indicates that although there is no clear effect of $AMFD$ strength on the spatial distribution of scaling clusters as shown in Fig. 7, the sign of moisture advection

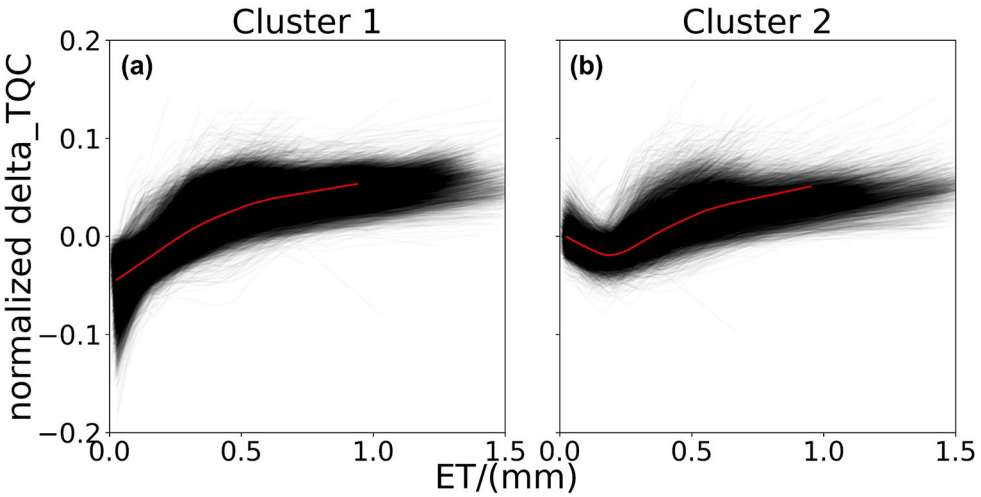

Fig. 6 Two distinct clusters of 3-hourly total ET and normalized $\Delta TQC/\Delta t$ (unitless) scaling curves were calculated over allgrid points using K-means clustering algorithm. Here is an example of clustering under the R_{wet} regime. The $\Delta TQC/\Delta t$ has been normalized for conducting K-means clustering on time series. The thick red lines represent the averaged scaling curve in one cluster and the black solid lines represent the grid-scale fitted scaling curves

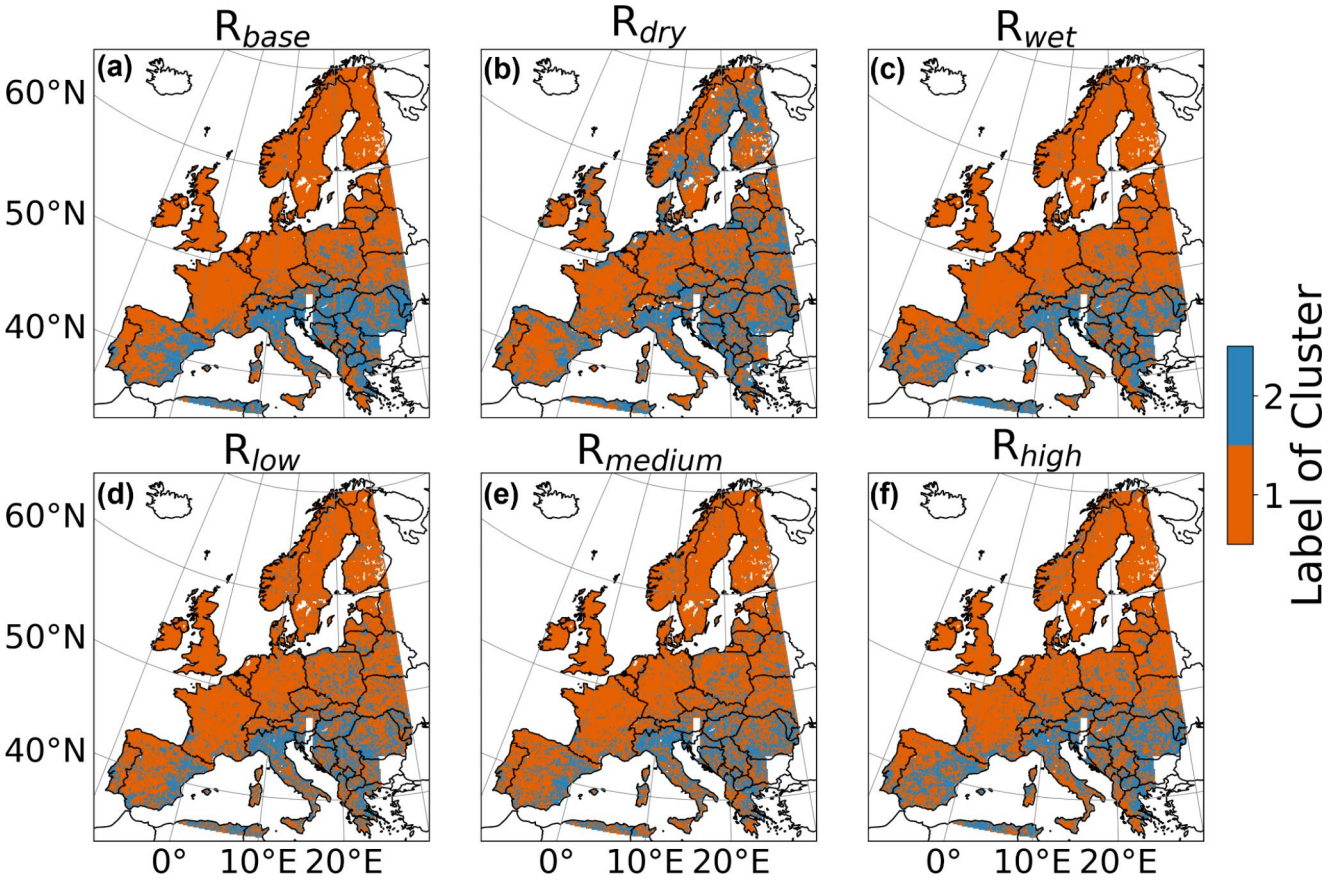

Fig. 7 Spatial distribution of the two types of scaling curves over all atmospheric regimes over the EURO-CORDEX region

can significantly change the scaling type between ET and $\Delta TQC/\Delta t$ at the grid point scale.

Under both R_{dry} and R_{wet}, the strongest TQC depletion (-0.1 mm/3 h) tends to occur when ET is lower than the 30% percentile and moisture flux divergence is higher than the 60% percentile. The highest $\Delta TQC/\Delta t$ occurs at high ET and strong moisture flux convergence under R_{wet}. For the R_{dry}, the highest $\Delta TQC/\Delta t$ occurs more frequently at the middle percentile of ET between 30 and 60%. The co-variability pattern of the $\Delta TQC/\Delta t$ distribution agrees well under R_{low} and R_{medium} as shown in Fig. S4. Compared to R_{dry}, with R_{wet}, the areas show either a strong decrease or an increase of $\Delta TQC/\Delta t$ both become much larger. For R_{wet}, the quantile phase plots between the PRUDENCE regions show a generally similar pattern, except for IP and AL, here the distribution of bins with high $\Delta TQC/\Delta t$ is more scattered under all atmospheric conditions. This is also observed in the cluster map, as these two regions show a spatial mix of the two types of scaling curves.

4 Discussion

4.1 Characteristics of ET and cloud water interaction

In this study, contrasting relationships were found between ET and the dynamic term ($\Delta TQC/\Delta t$) and storage term (TQC) of cloud water at the 3-hourly time scale in TSMP RCSM model results. The direct effect of ET is reflected in its positive contribution to the positive cloud water dynamics based on the scaling analysis. The positive scaling between ET and $\Delta TQC/\Delta t$ is similar to the well-known effect of *latent heat nudging* in data assimilation (Caldas-Alvarez and Khodayar 2020). The widespread negative scaling between ET and TQC over the EURO-CORDEX domain in Fig. 4 likely reflects a strong atmospheric control from net radiation that drives ET through atmospheric evaporative demand (Teuling et al. 2013). Under the R_{dry} or R_{low} regimes, the total cloud fraction is generally lower, as well as less cloud water, resulting overall in less atmospheric control with a low sensitivity between ET and TQC (Berg et al. 2015; Tao et al. 2019; Vogel et al. 2018), as indicated

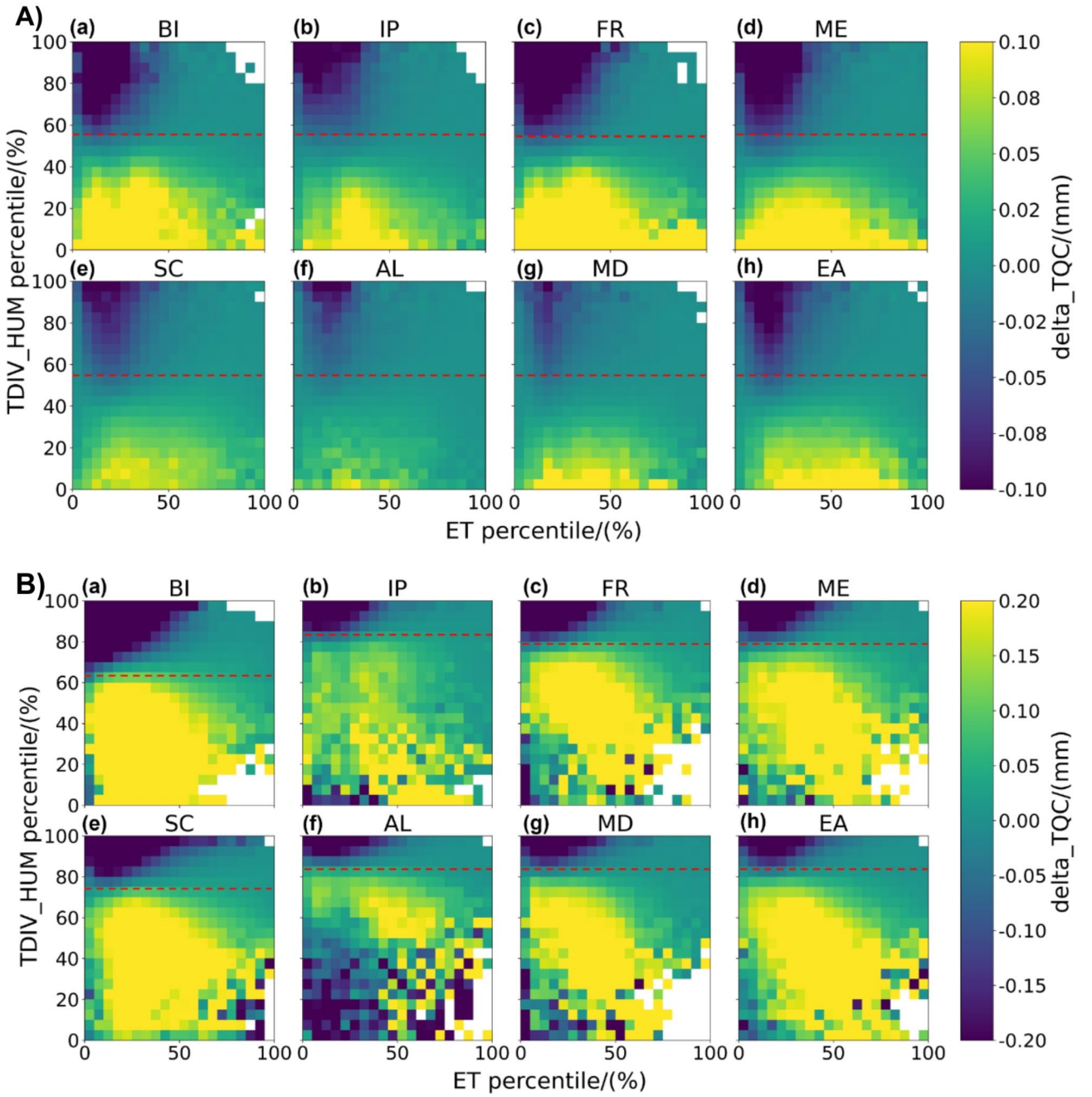

Fig. 8 Quantile phase plots of $\Delta TQC/\Delta t$ as a function of the percentile of ET and $TDIV\_HUM$ (using 10 percentile bins). Here, **A** represents the R_{dry} and **B** represents the R_{wet}. Subplots from a) to h) represent each PRUDENCE region respectively. The color in each bin represents the value of $\Delta TQC/\Delta t$ The strength of $AMFD$ is represented by the value of moisture flux divergence ($TDIV\_HUM$). A low percentile of $TDIV\_HUM$ represents strong convergence, while a high percentile represents strong divergence. The red dashed line indicates the percentile with almost zero $AMFD$

by a decrease in the correlation and a flatter curve of ET -TQC scaling in Figs. 2 and 4.

The spatial distribution of ET-TQC correlation (Fig. 2) shows a similar pattern to LH-SH in Fig. S1, where a positive correlation of LH -SH characterizes an energy-limited ET regime in humid regions and a negative correlation indicates a strong surface impact on the near-surface atmosphere due to water-limited ET, typically in transitional or dry regions (Fischer et al. 2007; Knist et al. 2017; Koster et al. 2004; Miralles et al. 2012; Seneviratne et al. 2006). Although the ET-TQC correlation analysis cannot directly demonstrate the directionality of coupling, its spatial pattern, analogous to the LH -SH relationship, may indirectly suggest a similar mechanism. Specifically, a lower ET-TQC correlation

could imply a stronger local land surface impact on TQC (Seneviratne et al. 2010).

However, the spatial distribution of ET-$\Delta TQC/\Delta t$ correlation is less consistent with the aforementioned analysis with weak correlation in IP and western MD as in Fig. 3a. This may be attributed to the dry conditions in summer that limit the generation of ET (Wei and Dirmeyer 2012), and the influence of the atmosphere is then more dominant than the local land surface states (Findell and Eltahir 2003b), despite of the water-limited strong coupling regime. Jach et al. 2020 classified the SM-Pr coupling regimes in Europe using the convective triggering potential (CTP)-low-level humidity index (HI_{low}) framework proposed by Findell and Eltahir (2003a) based on simulations. Northeastern and southeastern Europe are identified with the strongest land surface control on Pr as the water-limited transitional region, while the coupling strength is rather weak in both energy-limited wet regions like the Atlantic coast in west SC and BI, or water-limited dry regions like IP, which are classified as "atmospheric control" regions (Jach et al. 2020). Unlike the correlation relationship, the scaling relationships of ET-$\Delta TQC/\Delta t$ as shown in Fig. 5 are mostly modulated by the local ET regimes while their coupling strength tends to be stronger in dry and transitional areas under the water-limited regimes (Seneviratne et al. 2010). In general, the relationship between ET and cloud moisture could be a robust indicator of a L-A interaction diagnostic, because it can capture the spatial distribution pattern of L-A feedback as determined in previous studies in Europe (Knist et al. 2017; Jach et al. 2020).

In Fig. 7, it is also interesting to observe a clear hook scaling relationship as shown in Fig. 6 between ET and $\Delta TQC/\Delta t$ in southern (IP, MD) or eastern Europe (EA), known as dry and transitional regions (Knist et al. 2017). One working hypothesis about the hook structure is that since ET is under a water-limited regime in relatively dry regions, a very low ET implies an arid land surface as well as dry atmospheric conditions. Given an intensified thermal condition due to increased SH under low SM, a small increase in ET can moisten the atmosphere through local coupling, destabilizing the boundary layer (Liu et al. 2024; Su et al. 2023; Su et al. 2024), leading to accelerated cloud water depletion due to enhanced convective rain, resulting in the negative relationship between ET-$\Delta TQC/\Delta t$ as a hook structure. However, when ET further increases with SM, the ET regime gradually shifts into an energy-limited condition so the *PBL* becomes more stable so that the local moisture flux from ET cannot destabilize it. At the same time, the cloud water sink is compensated by the increased local moisture source from ET and the scaling again shows a logarithmic relationship. Therefore, the two types of scaling curves indicate that the responses to changes in TQC to ET are determined by the local ET regime, i.e. the evaporative fraction, as indicated by the similar distribution of LH-SH correlation in Fig. S1.

Similarly, the surface energy partitioning or ET regime defined by LH and SH has been used in previous studies to represent the L-A coupling strength (Knist et al. 2017). Their positive correlation indicates an energy-limited regime of ET in humid regions and a negative correlation by a strong surface control on the near-surface atmosphere due to water-limited ET in either transitional or dry regions, which further explains the distribution of the hooked scaling curves in water-limited regions in southern and eastern Europe and the responses of $\Delta TQC/\Delta t$ to ET modulated by the local ET regimes.

4.2 Effects of atmospheric aridity on ET and cloud water interaction

Many studies have discussed the effect of dry or wet soil on the L-A coupling from the perspective of the SM-Pr relationship; here convective precipitation initialization prefers dry soil due to the stronger local coupling by thermally induced vertical circulations generated by dry soil (Baur et al. 2018; Chen et al. 2020; Phillips and Klein 2014; Welty and Zeng 2018).

In this study, the role of atmospheric aridity is highlighted in that it can both directly impact L-A coupling by controlling the incoming net radiation, and indirectly intensify the control of SM on ET through the terrestrial leg by changing surface dryness, and ultimately affect the entire coupling chain and hence precipitation (Wei and Dirmeyer 2010). As discussed in Sect. 4.1, the ET-$\Delta TQC/\Delta t$ curves are limited by both SM and incoming radiation, based on the water- and energy-limited ET regimes, so the scalings could also be affected by both direct and indirect effects of atmospheric aridity. In Fig. 7 (b) and (c), for example, when comparing R_{wet} and R_{dry}, the hooked scaling relationships can also be detected in more humid areas such as BI and SC, where relationships shift from an energy-limited to a water-limited state due to the drying effect of the increased atmospheric aridity on the land surface. While the atmosphere is wet enough under $R_{wet,}$ the scaling relationships in these regions still follow the energy-limited logarithmic scaling. A decrease in the ET-TQC correlation coefficient under R_{dry} also indirectly reflects the increased surface control on the atmosphere and reduced limitation by incoming energy. Similarly, an increase in the local L-A coupling strength between ET and atmospheric variables was observed by Jach et al. 2022 and Schwitalla et al. 2023 in warm and dry summers in Europe.

Also, Dirmeyer et al. 2021 highlight the transition in ET regimes with intensified L-A coupling during the 2018

drought and heatwave in northern Europe, for example, in SC, which normally does not enter into such conditions, and the risk of this shift in exacerbating heatwaves and droughts. This regime shift is expected to be more frequent in the future, especially under high-emission climate scenarios. As a result, the proposed scaling analysis may serve as a valuable diagnostic tool in climate model projections. In this study, only total daily precipitation is however used to represent both SM drying and atmospheric drying; but high atmospheric aridity, for example, is not always associated with low soil moisture (Zhang et al. 2023). Future studies should explore the individual and combined effects of SM and atmospheric aridity on L-A interactions, particularly in the context of compound hot-dry events.

4.3 Effects of AMFD on ET and cloud water interaction

This study also investigates the effect of $AMFD$ on L-A feedbacks. *AMFD* can reduce the strength of the positive feedback between ET-$\Delta TQC/\Delta t$, and alter the scaling between ET and $\Delta TQC/\Delta t$ by providing a remote moisture source for cloud formation and changing the humidity of the atmosphere. This effect is most pronounced in the Atlantic coastal regions, including BI, SC, ME, FR, and IP, which have been identified as regions with strong atmospheric impacts by moisture advection from the ocean (Jach et al. 2020). Strong moisture flux advection provides a more stable boundary layer condition with a lower convective triggering potential so that surface moisture fluxes can hardly trigger cloud formation and precipitation events (Findell and Eltahir 2003b). Therefore, the relationship between surface moisture fluxes and atmospheric moisture becomes less strong. This could be the same mechanism behind the weak ET-$\Delta TQC/\Delta t$ coupling in this region. Moreover, the masking effect of $AMFD$ is less significant in R_{dry}, because the atmospheric moisture flux convergence is typically weaker than the divergence in the absence of precipitation so cloud water dynamics depend more on the local surface moisture flux than on remote moisture sources.

However, rather than looking at the absolute value of $AMFD$, its sign (convergence or divergence) can also contribute to the changes in atmospheric humidity and ultimately affect the scaling relationship between ET and $\Delta TQC/\Delta t$ as shown in Fig. 8. For example, a strong divergence can contribute to a drier condition that favors a hook scaling between ET and $\Delta TQC/\Delta t$. However, their effects cannot be discerned from Fig. 5 because the scaling curves here are averaged over the $AMFD$ range, which only shows the dominant effect of convergence or divergence at each region. Nevertheless, the large-scale $AMFD$ dominates in most events, with overall small local L-A feedbacks (Phillips and Klein 2014; Wei and Dirmeyer 2010). Tao et al. (2019) found that atmospheric moisture changes are more closely related to moisture flux convergence in dry years, while Ford et al. (2015) and Qing et al. (2023) also argued that remote moisture sources play a more important role in precipitation event initialization in dry regions. These discrepancies could be explained by the choice of target variables (cloud water vs. *Pr*) and the sensitivity of the time domain.

4.4 Limitations

While correlation analysis provides useful diagnostics for assessing the feedback between ET and cloud water, it cannot fully capture the causal direction inherent in these feedback processes without considering any time lag. In our context, the direction can only be estimated indirectly when evaluated together with well-established causal relationships, such as the LH-SH relationship (Seneviratne et al. 2010). The scaling analysis highlights a clear non-linearity between ET and cloud water as shown by the scaling curves in Figs. 5 and 6, given their coupling at 3 h. This again calls into question the robustness of linear metrics such as Pearson correlation in quantifying the strength of non-linear relationships in L-A feedback analysis. Correlation analysis can roughly capture the covariance between two variables but rarely provide valuable information on the functional relationships, as shown by the two distinct types of scaling relationships between ET and $\Delta TQC/\Delta t$. As L-A coupling is complex involving multiple variables and processes at different stages, rather a directional and multivariate method is required for a robust causality measurement, such as Peter-Clark Momentary Conditional Independence (PCMCI) algorithm or information theory methods (Krich et al. 2021; Hagan et al. 2022; Zhou et al. 2024).

Another limitation of the study is the problem of model dependence and its setup. The identified correlation and scaling relationships are highly dependent on the physics and parameterizations in the model. The use of an ensemble of RCMs could reduce the bias of the detected signal in any single model setup and increase the generalisability of the results. Furthermore, the observational dataset could be used as a reference for verification, as there are also discrepancies between observations and models for the mechanisms in cloud formation and the initialization of convective events by L-A feedback (Tao et al. 2021). Moreover, although.

TSMP closes the water and energy cycles from groundwater across the land surface to the top of the atmosphere, interactions between the land surface and atmosphere induced by the model coupling timestep of 900ss might be underestimated by the 3-hour resolution output. Nevertheless, the proposed diagnosis framework demonstrates the

robustness of TSMP RCSM simulations in simulating L-A interactions.

5 Conclusions

In this study, we analyzed L-A moisture flux feedbacks under different atmospheric conditions in the warm season based on TSMP simulations using correlation and binned-average scaling analysis, focusing on the relationship between ET and cloud water.

We found contrasting relationships: A negative correlation between ET-TQC indicates ET declines as the cloud moisture increases while the predominantly positive ET -$\Delta TQC/\Delta t$ scaling relationship highlights the role of surface moisture flux in influencing cloud moisture dynamics. The role of the ET regime in this feedback is also highlighted: the hotspots between ET - TQC feedback in Europe are mostly located in transitional zones in Eastern Europe and the Mediterranean, while the distribution of their scaling is determined by energy or water-limited ET regimes. Under R_{dry}, the shift of logarithmic scaling towards the hook scaling relationship in regions typically under an energy-limited regime indicates that a drier atmosphere can strengthen the local coupling by increasing the surface control on the atmosphere, while under R_{wet} there is a stronger atmospheric control on the surface variables due to the incoming energy as a constraint. The identified shift further reflects the potential effect of L-A coupling in intensifying hydrometeorological extreme events like droughts. In addition, $AMFD$ can reduce the strength of the positive feedback between ET-$\Delta TQC/\Delta t$ and affect their scaling relationships by providing remote moisture sources and changing the dry/wet atmospheric conditions.

In summary, our results highlight the role of cloud water in the atmospheric part of the L-A interaction and reveal the impact of different atmospheric conditions on L-A interaction. The proposed scaling analysis framework also demonstrates its advantages in accounting for the varying relationship between land and atmospheric variables over the sub-daily period. The identified non-linear scaling relationship of L-A interaction shows the limitations of common indices in representing the co-varying pattern of two variables, which calls for new metrics and tools for diagnosis.

Supplementary Information The online version contains supplementary material available at https://doi.org/10.1007/s00382-024-07475-w.

Acknowledgements The authors gratefully acknowledge: (i) The computing time granted by the JARA Vergabegremium and provided on the JARA Partition part of the supercomputer JURECA, and (ii) the Earth System Modelling Project (ESM) for funding this work by providing computing time on the ESM partition of the supercomputer JUWELS, both at Forschungszentrum Jülich (Jülich Supercomputing Centre, JSC).

Author contributions Conceptualization: Y. Zhang, N. Wagner, K. Goergen, S. Kollet; methodology: Y. Zhang, N. Wagner, K. Goergen, S. Kollet; formal analysis and investigation: Y. Zhang, K. Goergen, S. Kollet; writing - original draft preparation: Y. Zhang; writing - review and editing: Y. Zhang, K. Goergen, S. Kollet; funding acquisition: S. Kollet; supervision: K. Goergen, S. Kollet. All authors read and approved the final manuscript.

Funding Open Access funding enabled and organized by Projekt DEAL. This work has received funding from the Deutsche Forschungsgemeinschaft (DFG, German Research Foundation) – DETECT project SFB 1502/1–2022 – project number: 450058266.

Data availability The code for data pre-processing, statistical analysis, unsupervised learning, and visualization is available through GitHub. The dataset of TSMP-RCSM simulations is available as netCDF files and stored at a persistent data repository at Jülich Supercomputing Centre.

Declarations

Conflict of interest The authors have no relevant financial or non-financial interests to disclose.

References

Allan RP, Barlow M, Byrne MP, Cherchi A, Douville H, Fowler HJ, Gan TY, Pendergrass AG, Rosenfeld D, Swann ALS, Wilcox LJ, Zolina O (2020) Advances in understanding large-scale responses of the water cycle to climate change. Ann N Y Acad Sci 1472(1):49–75. https://doi.org/10.1111/nyas.14337

Baldauf M, Seifert A, Förstner J, Majewski D, Raschendorfer M, and Thorsten Reinhardt (2011) Operational convective-scale Numerical Weather Prediction with the COSMO Model: description and sensitivities. Mon Weather Rev 139(12):3887–3905. https://doi.org/10.1175/MWR-D-10-05013.1

Baur F, Keil C, Craig GC (2018) Soil moisture–precipitation coupling over Central Europe: interactions between Surface anomalies at different scales and the Dynamical Implication. Q J R Meteorol Soc 144(717):2863–2875. https://doi.org/10.1002/qj.3415

Bechtold P, Köhler M, Jung T, Doblas-Reyes F, Leutbecher M, Rodwell MJ, Vitart F, and Gianpaolo Balsamo (2008) Advances in simulating Atmospheric variability with the ECMWF Model: from synoptic to Decadal Time-Scales. Q J R Meteorol Soc 134(634):1337–1351. https://doi.org/10.1002/qj.289

Berg A, Lintner BR, Findell K, Seneviratne SI, Bart, van den Hurk Chéruy F, et al (2015) Interannual Coupling between Summertime Surface Temperature and Precipitation over Land: Processes and Implications for Climate Change. J Climate 28(3):1308–28. https://doi.org/10.1175/JCLI-D-14-00324.1

Berg A, Lintner BR, Findell K, and Alessandra Giannini (2017) Uncertain Soil Moisture feedbacks in Model projections of Sahel Precipitation. Geophys Res Lett 44(12):6124–6133. https://doi.org/10.1002/2017GL073851

Betts AK, Desjardins R, Beljaars ACM, and Ahmed Tawfik (2015) Observational study of Land-Surface-Cloud-Atmosphere Coupling on Daily timescales. Front Earth Sci 3. https://www.frontiersin.org/articles/10.3389/feart.2015.00013

Caldas-Alvarez A, and Samiro Khodayar (2020) Assessing Atmospheric Moisture effects on Heavy Precipitation during HyMeX IOP16 using GPS nudging and dynamical downscaling. Nat Hazards Earth Syst Sci 20(10):2753–2776. https://doi.org/10.5194/nhess-20-2753-2020

Chen J, Hagos S, Xiao H, Fast JD, and Zhe Feng (2020) Characterization of Surface Heterogeneity-Induced Convection using cluster analysis. J Geophys Research: Atmos 125(20). https://doi.org/10.1029/2020JD032550. e2020JD032550

Christensen J, Hesselbjerg, Ole Bøssing C (2007) A Summary of the PRUDENCE model projections of changes in European climate by the end of this century. Clim Change 81(1):7–30. https://doi.org/10.1007/s10584-006-9210-7

Dirmeyer PA (2011) The terrestrial segment of Soil moisture–climate coupling. Geophys Res Lett 38(16). https://doi.org/10.1029/2011GL048268

Dirmeyer PA, Jin Y, Singh B, and Xiaoqin Yan (2013a) Evolving land–atmosphere interactions over North America from CMIP5 simulations. J Clim 26(19):7313–7327. https://doi.org/10.1175/JCLI-D-12-00454.1

Dirmeyer PA, Jin Y, Singh B, and Xiaoqin Yan (2013b) Trends in land–atmosphere interactions from CMIP5 simulations. J Hydrometeorol 14(3):829–849. https://doi.org/10.1175/JHM-D-12-0107.1

Dirmeyer PA, Balsamo G, Blyth EM, Morrison R (2021) and Hollie M. Cooper. Land-Atmosphere Interactions Exacerbated the Drought and Heatwave Over Northern Europe During Summer 2018. *AGU Advances* 2 (2): e2020AV000283. https://doi.org/10.1029/2020AV000283

Dominguez F, and Praveen Kumar (2008) Precipitation recycling variability and Ecoclimatological Stability—A Study using NARR Data. Part I: Central U.S. Plains Ecoregion. J Clim 21(20):5165–5186. https://doi.org/10.1175/2008JCLI1756.1

Doms G, Schattler U n.d. A Description of the Nonhydrostatic Regional Model LM

Doms G, Förstner J, Heise E, Reinhardt T, Ritter B, Schrodin R n.d. A Description of the Nonhydrostatic Regional COSMO-Model

Findell KL, Elfatih AB, Eltahir (2003a) Atmospheric controls on Soil moisture–boundary layer interactions. Part I: Framework Development. J Hydrometeorol 4(3):552–569. https://doi.org/10.1175/1525-7541(2003)004<0552:ACOSML>2.0.CO;2

Findell KL, Elfatih AB, Eltahir (2003b) Atmospheric controls on Soil moisture–boundary layer interactions. Part II: feedbacks within the Continental United States. J Hydrometeorol 4(3):570–583. https://doi.org/10.1175/1525-7541(2003)004<0570:ACOSML>2.0.CO;2

Findell KL, Yin Z, Seo E, Dirmeyer PA, Arnold NP, Chaney N, Fowler MD et al (2024) Accurate Assessment of Land–Atmosphere Coupling in Climate models requires high-frequency data output. Geosci Model Dev 17(4):1869–1883. https://doi.org/10.5194/gmd-17-1869-2024

Fischer EM, Seneviratne SI, Vidale PL, Lüthi D, Schär C (2007) Soil moisture–atmosphere interactions during the 2003 European Summer Heat Wave. J Clim 20(20):5081–5099. https://doi.org/10.1175/JCLI4288.1

Ford TW, Anita D, Rapp, Quiring SM (2015) Does Afternoon Precipitation Occur preferentially over dry or wet soils in Oklahoma? J Hydrometeorol 16(2):874–888. https://doi.org/10.1175/JHM-D-14-0005.1

Furusho-Percot C, Goergen K, Hartick C, Kulkarni K, Keune J, and Stefan Kollet (2019) Pan-european Groundwater to Atmosphere Terrestrial systems Climatology from a physically consistent Simulation. Sci Data 6(1):320. https://doi.org/10.1038/s41597-019-0328-7

Furusho-Percot C, Goergen K, Hartick C, Poshyvailo-Strube L, Kollet S (2022) Groundwater Model impacts Multiannual simulations of Heat waves. Geophys Res Lett 49(10). https://doi.org/10.1029/2021GL096781. e2021GL096781

Gasper F, Goergen K, Shrestha P, Sulis M, Rihani J, Geimer M, Kollet S (2014) Implementation and scaling of the fully coupled Terrestrial systems modeling platform (TerrSysMP v1.0) in a massively parallel supercomputing environment – a case study on JUQUEEN (IBM Blue Gene/Q). Geosci Model Dev 7(5):2531–2543. https://doi.org/10.5194/gmd-7-2531-2014

Hagan DFT, Han AJ, Dolman G, Wang, Kenny TC, Lim Kam Sian K, Yang W, Ullah, Shen R (2022) Contrasting ecosystem constraints on Seasonal Terrestrial CO2 and Mean Surface Air Temperature Causality projections by the end of the 21st Century. Environ Res Lett 17(12):124019. https://doi.org/10.1088/1748-9326/aca551

Hersbach H, Bell B, Berrisford P, Hirahara S et al (2020) András Horányi, Joaquín Muñoz-Sabater, Julien Nicolas,. The ERA5 Global Reanalysis. Q J R Meteorol Soc 146(730):1999–2049. https://doi.org/10.1002/qj.3803

Jach L, Warrach-Sagi K, Ingwersen J, Kaas E, and Volker Wulfmeyer (2020) Land Cover impacts on Land-Atmosphere Coupling Strength in Climate simulations with WRF over Europe. J Geophys Research: Atmos 125(18). https://doi.org/10.1029/2019JD031989. e2019JD031989

Jach L, Schwitalla T, Branch O, Warrach-Sagi K, and Volker Wulfmeyer (2022) Sensitivity of land–atmosphere coupling strength to changing Atmospheric temperature and moisture over Europe. Earth Sys Dyn 13(1):109–132. https://doi.org/10.5194/esd-13-109-2022

Jones JE, Woodward CS (2001) Newton–Krylov-Multigrid solvers for Large-Scale, highly heterogeneous, variably saturated Flow problems. Adv Water Resour 24(7):763–774. https://doi.org/10.1016/S0309-1708(00)00075-0

Knist S, Goergen K, Buonomo E, Bøssing O, Christensen A, Colette RM, Cardoso R, Fealy et al (2017) Land-Atmosphere Coupling in EURO-CORDEX evaluation experiments. J Geophys Research: Atmos 122(1):79–103. https://doi.org/10.1002/2016JD025476

Kollet SJ, and Reed M. Maxwell (2006) Integrated Surface–Groundwater Flow modeling: a free-surface Overland Flow Boundary Condition in a parallel Groundwater Flow Model. Adv Water Resour 29(7):945–958. https://doi.org/10.1016/j.advwatres.2005.08.006

Koster RD, Dirmeyer PA, Guo Z, Bonan G, Chan E, Cox P, Gordon CT et al (2004) Regions of strong coupling between soil moisture and precipitation. Science 305(5687):1138–1140. https://doi.org/10.1126/science.1100217

Kotthaus S, Sue C, Grimmond B (2018) Atmospheric Boundary-Layer characteristics from Ceilometer measurements. Part 1: a new method to track mixed Layer Height and Classify clouds. Q J R Meteorol Soc 144(714):1525–1538. https://doi.org/10.1002/qj.3299

Krich C, Migliavacca M, Miralles DG, Kraemer G, Tarek S, El-Madany M, Reichstein J, Runge, and Miguel D. Mahecha (2021) Functional convergence of biosphere–atmosphere interactions in response to Meteorological conditions. Biogeosciences 18(7):2379–2404. https://doi.org/10.5194/bg-18-2379-2021

Liu X, He B, Guo L, Huang L, Chen D (2020) Similarities and differences in the mechanisms causing the European summer heatwaves in 2003, 2010, and 2018. Earth's Future 8(4). https://doi.org/10.1029/2019EF001386. e2019EF001386

Liu W, Yue P, Wu X, Li J, Shao N, Zhu B (2024) and Chunsong Lu. Why Does a Decrease in Cloud Amount Increase Terrestrial Evapotranspiration in a Monsoon Transition Zone? *Environmental Research Letters*, March. https://doi.org/10.1088/1748-9326/ad3569

Maxwell RM (2013) A terrain-following Grid transform and preconditioner for parallel, Large-Scale, Integrated Hydrologic modeling. Adv Water Resour 53(March):109–117. https://doi.org/10.1016/j.advwatres.2012.10.001

Miralles DG, van den Berg MJ, Teuling AJ, de a. R (2012) Jeu. Soil Moisture-Temperature Coupling: A Multiscale Observational Analysis. Geophys Res Lett 39(21). https://doi.org/10.1029/2012GL053703

Oleson KW, Niu G-Y, Yang Z-L, Lawrence DM, Thornton PE, Lawrence PJ, Stöckli R et al (2008) Improvements to the Community Land Model and their impact on the Hydrological cycle. J Geophys Research: Biogeosciences 113(G1). https://doi.org/10.1029/2007JG000563

Phillips TJ, Klein SA (2014) Land-Atmosphere Coupling manifested in warm-season observations on the U.S. Southern Great Plains. J Geophys Research: Atmos 119(2):509–528. https://doi.org/10.1002/2013JD020492

Qing Y, Wang S, Yang Z-L, and Pierre Gentine (2023) Soil moisture–atmosphere Feedbacks have triggered the shifts from Drought to Pluvial conditions since 1980. Commun Earth Environ 4(1):1–10. https://doi.org/10.1038/s43247-023-00922-2

Santanello JA, Christa D, Peters-Lidard, Kumar SV (2011) Diagnosing the sensitivity of local land–atmosphere Coupling via the Soil moisture–boundary Layer Interaction. J Hydrometeorol 12(5):766–786. https://doi.org/10.1175/JHM-D-10-05014.1

Santanello JA, Dirmeyer PA, Ferguson CR, Findell KL, Tawfik AB, Berg A, Ek M et al (2018) Land–atmosphere interactions: the LoCo Perspective. Bull Am Meteorol Soc 99(6):1253–1272. https://doi.org/10.1175/BAMS-D-17-0001.1

Schwitalla T, Jach L, Wulfmeyer V (2023) and Kirsten Warrach-Sagi. Soil Moisture-Atmosphere Coupling Strength over Central Europe in the Recent Warming Climate. Preprint. Atmospheric, Meteorological and Climatological Hazards. https://doi.org/10.5194/egusphere-2023-1725

Sedlar J, Riihimaki LD, Turner DD, Duncan J, Adler B, Bianco L, Lantz K et al (2022) Investigating the impacts of Daytime Boundary Layer clouds on Surface Energy fluxes and Boundary Layer structure during CHEESEHEAD19. J Geophys Research: Atmos 127(5). https://doi.org/10.1029/2021JD036060. e2021JD036060

Seneviratne SI, Lüthi D, Litschi M, Schär C (2006) Land–atmosphere Coupling and Climate Change in Europe. Nature 443(7108):205–209. https://doi.org/10.1038/nature05095

Seneviratne SI, Corti T, Davin EL, Hirschi M, Jaeger EB, Lehner I, Orlowsky B, Adriaan JT (2010) Investigating soil moisture–climate interactions in a changing climate: a review. Earth Sci Rev 99(3):125–161. https://doi.org/10.1016/j.earscirev.2010.02.004

Shrestha P, Sulis M, Masbou M, Kollet S, Simmer C (2014) A scale-consistent Terrestrial systems modeling platform based on COSMO, CLM, and ParFlow. Mon Weather Rev 142(9):3466–3483. https://doi.org/10.1175/MWR-D-14-00029.1

Su T, Li Z, and Youtong Zheng (2023) Cloud-surface coupling alters the morning transition from stable to unstable boundary layer. Geophys Res Lett 50(5). https://doi.org/10.1029/2022GL102256. e2022GL102256

Su H, Yang Z-L, Dickinson RE, and Jiangfeng Wei (2014) Spring Soil moisture-precipitation feedback in the Southern Great Plains: how is it related to large-Scale Atmospheric conditions? Geophys Res Lett 41(4):1283–1289. https://doi.org/10.1002/2013GL058931

Su T, Li Z, Zhang Y, Zheng Y, Zhang H (2024) Observation and Reanalysis Derived relationships between Cloud and Land Surface fluxes Across Cumulus and Stratiform Coupling over the Southern Great Plains. Geophys Res Lett 51(8). https://doi.org/10.1029/2023GL108090. e2023GL108090

Tao C, Zhang Y, Tang S, Tang Q, Ma H-Y, Xie S, and Minghua Zhang (2019) Regional Moisture Budget and Land-Atmosphere Coupling over the U.S. Southern Great Plains inferred from the ARM Long-Term observations. J Geophys Research: Atmos 124(17–18):10091–10108. https://doi.org/10.1029/2019JD030585

Tao C, Zhang Y, Tang Q, Ma H-Y, Ghate VP, Tang S, Xie S, Santanello JA (2021) Land–atmosphere coupling at the U.S. Southern Great Plains: a comparison on local convective regimes between ARM observations, reanalysis, and Climate Model simulations. J Hydrometeorol 22(2):463–481. https://doi.org/10.1175/JHM-D-20-0078.1

Taylor C, de Jeu R, Guichard F et al (2012) Afternoon rain more likely over drier soils. Nature 489:423–426. https://doi.org/10.1038/nature11377

Tesch T, Kollet S, and Jochen Garcke (2023) Causal deep learning models for studying the Earth System. Geosci Model Dev 16(8):2149–2166. https://doi.org/10.5194/gmd-16-2149-2023

Teuling AJ, Anne F, Van Loon SI, Seneviratne I, Lehner M, Aubinet B, Heinesch C, Bernhofer T, Grünwald H, Prasse, Spank U (2013) Evapotranspiration amplifies European Summer Drought. Geophys Res Lett 40(10):2071–2075. https://doi.org/10.1002/grl.50495

Tian J, Zhang Y, Klein SA, Öktem R, Wang L (2022) How does Land Cover and its heterogeneity length scales affect the formation of summertime shallow Cumulus clouds in observations from the US Southern Great Plains? Geophys Res Lett 49(7). https://doi.org/10.1029/2021GL097070. e2021GL097070

Tiedtke M (1989) A Comprehensive Mass Flux Scheme for Cumulus parameterization in large-scale models. August. https://journals.ametsoc.org/view/journals/mwre/117/8/1520-0493_1989_117_1779_acmfsf_2_0_co_2.xml

Valcke S (2013) The OASIS3 coupler: a European Climate Modelling Community Software. Geosci Model Dev 6(2):373–388. https://doi.org/10.5194/gmd-6-373-2013

Vogel MM, Zscheischler J, Sonia I, Seneviratne (2018) Varying soil moisture–atmosphere feedbacks explain divergent temperature extremes and precipitation projections in Central Europe. Earth Sys Dyn 9(3):1107–1125. https://doi.org/10.5194/esd-9-1107-2018

Wang Y, Li R, Hu J, Fu Y, Duan J, Cheng Y, and Binbin Song (2021) Understanding the non-linear response of summer evapotranspiration to clouds in a Temperate Forest under the impact of Vegetation Water Content. J Geophys Research: Atmos 126(23). https://doi.org/10.1029/2021JD035239. e2021JD035239

Wang Y, Li R, Song B, and Jiheng Hu (2024) Divergent responses of summer terrestrial evapotranspiration to Cloud increase in East Asia. J Geophys Research: Atmos 129(6). https://doi.org/10.1029/2023JD039246. e2023JD039246

Wei J, Dirmeyer PA (2010) Toward understanding the large-Scale Land-Atmosphere Coupling in the models: roles of different processes. Geophys Res Lett 37(19). https://doi.org/10.1029/2010GL044769

Wei J, Dirmeyer PA (2012) Dissecting soil moisture-precipitation coupling. Geophys Res Lett 39(19). https://doi.org/10.1029/2012GL053038

Welty J, Zeng X (2018) Does Soil Moisture affect warm season precipitation over the Southern Great Plains? Geophys Res Lett 45(15):7866–7873. https://doi.org/10.1029/2018GL078598

Zängl Günther, Reinert D, Rípodas P, and Michael Baldauf (2015) The ICON (ICOsahedral Non-hydrostatic) Modelling Framework of

DWD and MPI-M: description of the non-hydrostatic dynamical core. Q J R Meteorol Soc 141(687):563–579. https://doi.org/10.1002/qj.2378

Zhang W, Koch J, Wei F, Zeng Z, Fang Z, and Rasmus Fensholt (2023) Soil Moisture and Atmospheric Aridity Impact Spatio-temporal changes in Evapotranspiration at A Global Scale. J Geophys Research: Atmos 128(8). https://doi.org/10.1029/2022JD038046. e2022JD038046

Zhou F, Hagan DFT, Wang G, San Liang X, Li S, Shao Y, Yeboah E (2024) and Xikun Wei. Estimating Time-Dependent Structures in a Multi-Variate Causality for Land-Atmosphere Interactions. J Climate 1 (aop). https://doi.org/10.1175/JCLI-D-23-0207.1

Zhou S, Williams AP, Lintner BR et al (2021) Soil moisture–atmosphere feedbacks mitigate declining water availability in drylands. Nat Clim Chang 11:38–44. https://doi.org/10.1038/s41558-020-00945-z